THE EMPIRICAL VALIDATION OF A MODEL FOR SMALL-SCALE FUEL-CELL COGENERATION SYSTEMS

Ian Beausoleil-Morrison
CANMET Energy Technology Centre, Natural Resources Canada, Ottawa Canada

ABSTRACT

A mathematical model has been developed for simulating the performance of small-scale fuel-cell cogeneration systems. An experimental programme has been conducted to calibrate the model (i.e. establish its inputs) to simulate the performance of a prototype solid-oxide fuel-cell system. Data from a disjunct set of experiments were used to empirically validate this model and its calibration. Despite the challenges in calibrating some terms which are significant to the model's energy balances and despite some internally inconsistent measurements, comparisons between model predictions and quantities derived from the measurements were found to range from acceptable to excellent. Agreement was found to be best for aspects of the model that could be isolated in the simpler comparisons while agreement was less satisfactory when examining parameters that required the concurrent operation of all aspects of the model.

KEYWORDS

Fuel cell cogeneration, empirical validation.

INTRODUCTION

Small-scale (< 10 kW) cogeneration—the concurrent production of electricity and heat from a single fuel source—is an emerging technology with the potential to reduce energy consumption and GHG emissions. The decentralized production of electricity could also reduce electrical transmission and distribution congestion and alleviate utility peak demand problems. A number of manufacturers worldwide are developing natural-gas-fired cogeneration devices for single-family and multi-family residential buildings based upon fuel cells, internal combustion engines, and Stirling engines (Knight and Ugursal, 2005) while adoption of the technology is being encouraged by energy utilities (e.g. Powergen in UK; Tokyo Gas in Japan) and by favourable electricity tariff structures (e.g. the German Combined Heat and Power Act).

These small-scale cogeneration devices have only modest electrical conversion efficiencies: ∼10-35% of the source fuel's lower heating value (LHV). Consequently, the effective exploitation of the cogeneration device's thermal output for space heating, space cooling, and/or heating domestic hot water is crucial if high levels of overall energy efficiency and the associated environmental benefits are to be realized. Given this strong coupling between the cogeneration device and the building, it is necessary to incorporate models of cogeneration devices into whole-building simulation in order to provide answers to significant questions on the applicability and impact of the technology, such as:

- What are the net energy and GHG impacts?
- What combinations of building envelope, occupancy pattern, and climate are favourable for cogeneration?
- What are the optimal dispatch strategies?
- How should the building's thermal plant be configured to maximally exploit the thermal output?
- What are the appropriate electrical generation and thermal storage capacities?

These factors motivated the formation of Annex 42 of the International Energy Agency's Energy Conservation in Buildings and Community Systems Programme (IEA/ECBCS). This international collaborative project aims to develop, validate, and implement models of cogeneration devices for whole-building simulation programs. IEA/ECBCS Annex 42 has developed a mathematical model for simulating the performance of fuel cell cogeneration systems (Beausoleil-Morrison et al., 2006b). This is a system-level model that considers the thermodynamic performance of all components that consume energy and produce thermal and electrical output. The model relies heavily upon empirical information that can be acquired from the testing of coherent systems or components and is designed for operation at a time resolution in the order of minutes.

An experimental programme has been conducted with a prototype solid-oxide fuel-cell (SOFC) cogeneration system. This consisted of a series of experiments with varied and controlled boundary conditions. The experiments were segregated into two groups:

- 45 *calibration* experiments which yielded data that were used to calibrate the model (i.e. establish its inputs) to represent this specific device.
- 16 *validation* experiments.

The current paper treats the validation of the mathematical model and the accuracy of its calibration using the empirical data gathered from the validation experiments. A brief review of pertinent aspects of the mathematical model is first provided, followed by a concise presentation of the model's calibration to represent the prototype SOFC device. The majority of the paper is dedicated to comparisons between simulations conducted with the calibrated model and measurements from the validation experiments. Concluding remarks are then provided along with recommendations for future work.

MODEL DESCRIPTION

The IEA/ECBCS Annex 42 fuel cell cogeneration model is based upon an energy balance approach. For reasons of extensibility and adaptability it discretizes the cogeneration system's components into control volumes

that produce electrical power, supply air, capture heat from the hot product gases, etc. Energy balances are formed and solved for each control volume on a time-step basis, this to accurately treat the interactions with the building, the occupants, and control systems. Each control volume is modelled in as rigorous a fashion as possible given the constraints of computational efficiency and the need to calibrate model inputs based upon the testing of coherent systems.

Energy balances

The fuel cell's stack, reformer, and afterburner are represented by a control volume known as the fuel cell power module (FCPM). Its energy balance can be written in the following form,

$$\dot{H}_{fuel} + \dot{H}_{air} = P_{el} + \dot{H}_{FCPM-cg} + q_{skin-loss} + q_{FCPM-to-dilution} \quad (1)$$

Where $\dot{H}_{fuel}$ and $\dot{H}_{air}$ represent the enthalpy carried into the control volume by fuel and air (for electrochemical and combustion reactions as well as excess air). P_{el} is the net DC power production, that is the stack power less ohmic losses in cabling and the power draw of ancillaries (e.g. the fan that supplies the air). $\dot{H}_{FCPM-cg}$ represents the enthalpy carried out of the control volume by the exiting gas stream (the products of the electrochemical and combustion reactions as well as the excess air and the inert constituents of the fuel). The final two terms in equation 1 represent thermal losses: $q_{skin-loss}$ is the radiant and convective heat transfer to the containing room while $q_{FCPM-to-dilution}$ represents the heat transfer from the FCPM to the air stream which is drawn through the cogeneration device's cabinet to comply with gas venting requirements of safety codes.

The thermal energy of the FCPM's hot exhaust gases (represented by the $\dot{H}_{FCPM-cg}$ term in equation 1) is transferred through a heat exchanger to a water loop connected to the building's plant. This provides the cogeneration device's useful thermal output (q_{HX}). This heat transfer is characterized with the log mean temperature difference (LMTD) method for counterflow heat exchangers[1],

$$q_{HX} = (UA)_{eff} \cdot \frac{(T_{FCPM-cg} - T_{w-out}) - (T_{g-out} - T_{w-in})}{ln\left(\frac{T_{FCPM-cg} - T_{w-out}}{T_{g-out} - T_{w-in}}\right)} \quad (2)$$

Where $T_{FCPM-cg}$ is the temperature of the hot gases exiting the FCPM and entering the heat exchanger and T_{g-out} is the temperature of the cooled gases exiting the heat exchanger. T_{w-in} is the temperature of the cold water at the heat exchanger inlet and T_{w-out} is the temperature of the warmed water exiting the heat exchanger. $(UA)_{eff}$ is the effective product of the heat transfer coefficient and area (W/K).

A power conditioning system converts the FCPM's DC output to AC power to supply the building's electrical loads and perhaps to export power to the grid. A simple energy balance is used to represent the control volume for this device,

$$P_{AC} = \eta_{PCU} \cdot P_{el} \quad (3)$$

Where P_{AC} represents the cogeneration device's AC power production and η_{PCU} is the DC-AC power conversion efficiency.

Equations 1 through 3 outline the methods used to characterize the energy balances for three of the model's control volumes. Similar techniques are employed for the remaining six control volumes.

Empirical coefficients

There is a great deal of interdependency between the nine energy balances and the individual terms of the energy balances. For example, the net DC power production (appearing in equations 1 and 3) is related to the fuel consumption (and thus the $\dot{H}_{fuel}$ term of equation 1) through the FCPM's electrical efficiency,

$$\varepsilon_{el} = \frac{P_{el}}{\dot{N}_{fuel} \cdot LHV_{fuel}} \quad (4)$$

Where ε_{el} is the electrical efficiency and $\dot{N}_{fuel}$ is the molar flow rate of the fuel.

Many of the individual terms of the energy balances are empirical in nature and are evaluated on a time-step basis. For example, the FCPM's electrical efficiency required by equation 4 is given by[2],

$$\varepsilon_{el} = \varepsilon_0 + \varepsilon_1 \cdot P_{el} + \varepsilon_2 \cdot P_{el}^2 \quad (5)$$

Where ε_i are empirical coefficients.

Similarly, $(UA)_{eff}$ required in equation 2 is expressed as a parametric relation of the water ($\dot{N}_w$) and gas ($\dot{N}_g$) flow rates through the heat exchanger,

$$(UA)_{eff} = hx_{s,0} + hx_{s,1} \cdot \dot{N}_w + hx_{s,2} \cdot \dot{N}_w^2 + hx_{s,3} \cdot \dot{N}_g + hx_{s,4} \cdot \dot{N}_g^2 \quad (6)$$

Where $hx_{s,i}$ are empirical coefficients.

The DC-AC power conditioning efficiency is given by,

$$\eta_{PCU} = u_0 + u_1 \cdot P_{el} + u_2 \cdot P_{el}^2 \quad (7)$$

Where u_i are empirical coefficients.

Expressions similar to equations 5 through 7 are used to evaluate many of the other terms in the energy balances on a time-step basis.

Solution procedure

At each time-step of a simulation, the building simulation program invokes the fuel cell cogeneration model and passes it a control signal requesting a given AC power output (P_{AC}). The fuel cell's operating point is

[1] A more complex approach is employed when conditions are such that water vapour in the gas stream can condense.

[2] Equation 5 also contains terms that express degradation as a result of operational time and stop-start cycling, but these are omitted here for the sake of clarity.

established by determining the FCPM's net DC power production (P_{el}) through solution of equations 7 and 3. The electrical efficiency (ε_{el}) is calculated with equation 5 and the required fuel consumption ($\dot{N}_{fuel}$) determined with equation 4. A polynomial expression is used to estimate the enthalpy of each fuel constituent (CH_4, C_2H_6, N_2, etc.) as a function of its supply temperature. This along with $\dot{N}_{fuel}$ establishes the first term of the equation 1 energy balance. Clearly, any errors in the evaluation of equations 3, 4, 5, and 7 or in the ε_i or u_i empirical coefficients will lead to errors in the determination of the fuel consumption.

Similar methods are used to establish the other terms of equation 1, which is then solved to yield the enthalpy carried out of the control volume by the gas stream ($\dot{H}_{FCPM-cg}$). The composition of this gas stream is determined by assuming complete reactions between the fuel constituents and the air's O_2,

$$C_xH_y + \left(x + \tfrac{y}{4}\right) \cdot O_2 \rightarrow x \cdot CO_2 + \tfrac{y}{2} \cdot H_2O \qquad (8)$$

When the results of equation 8 are added to the flow rates of the non-reacting fuel and air constituents, the composition and flow rate ($\dot{N}_g$) of the product gas stream are established. The polynomial function mentioned above is then applied in an iterative manner to establish the temperature ($T_{FCPM-cg}$) corresponding to the value of $\dot{H}_{FCPM-cg}$ solved by equation 1. Clearly, any errors in the evaluation of any of the above-mentioned equations (and others not mentioned here) or any errors in their empirical coefficients would lead to errors in the estimate of $T_{FCPM-cg}$.

This temperature is then used in the modelling of the heat exchanger. Firstly, the flow rate of the product gas stream ($\dot{N}_g$) is used to establish $(UA)_{eff}$ using equation 6. A re-arrangement of equation 2 is then solved to determine the cogeneration device's useful thermal output (q_{HX}) and the heat exchanger's exiting gas and water temperatures. Once again, any errors in the evaluation of the many terms that lead to $\dot{N}_g$ and $T_{FCPM-cg}$ will propagate into errors in the prediction of q_{HX}.

MODEL CALIBRATION

The previous section outlined some of the model's equations requiring empirical coefficients (5, 6, and 7). These coefficients are the model's inputs. The form of these empirical equations was chosen to facilitate model calibration based upon the testing of coherent fuel cell cogeneration systems. The calibration process essentially involves the design and execution of experiments that isolate the performance of specific aspects of the cogeneration system. Quantities are derived from the measured data and regressions performed to establish the empirical coefficients.

As mentioned in the paper's introduction, such a calibration has been performed for a prototype cogeneration system. The experimental configuration, types of instrumentation employed, operating scenarios examined, uncertainty analysis, and regression methods are detailed in Beausoleil-Morrison et al. (2006c).

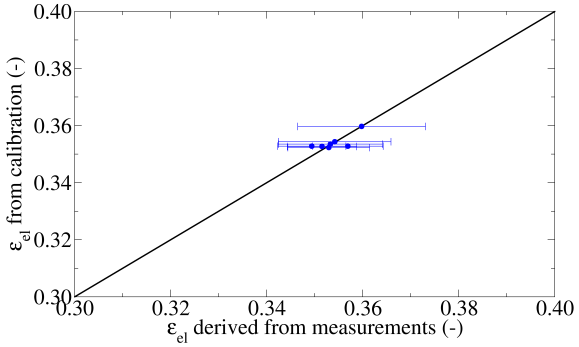

Figure 1: Equation 5 versus measurements for calibration experiments

Figure 1 illustrates this effort's calibration of equation 5. Seven experiments were performed over a range of P_{el}. For each of these 7 experiments, the value of P_{el} was derived from two voltage measurements and two current measurements (one pair to establish the stack power production less cabling ohmic losses and the other the DC power draw of ancillaries). These derived P_{el} values along with measurements of $\dot{N}_{fuel}$ were used to evaluate equation 4 to derive the value of ε_{el} for each of the 7 experiments. The value of LHV_{fuel} required by equation 4 was derived from the fuel's composition as determined through gas chromatography. The ε_{el} values derived from the measurements are plotted along the figure's x-axis. The error bars represent the uncertainty at the 95% confidence level, as determined by propagating instrument bias errors and precision indices using the method described by Moffat (1988).

The experiments resulted in 7 pairs of derived ε_{el} and P_{el} values. A non-linear regression of equation 5 was performed with these data to yield the calibrated ε_i empirical coefficients. The ε_{el} subsequently determined with equation 5 using these ε_i coefficients are plotted on the y-axis of Figure 1. Essentially this figure examines the ability of equation 5 and the calibrated ε_i coefficients to represent the data from which the coefficients were derived. Table 1 presents the average deviation (error) in ε_{el} between the calibration and the values derived from the measurements from the 7 experiments. It also presents the root-mean-square (rms) and the maximum errors.

This calibration procedure was repeated for all terms pertinent to this SOFC system[3]. Figure 2 illustrates the calibration of one of these other terms, $q_{FCPM-to-dilution}$ which is treated as a constant value in the model. The uncertainty associated with this derived quantity is significant, for reasons explained in Beausoleil-Morrison et al. (2006c). The goodness-of-fit metrics for the calibration of each term are given in Table 1. An estimated

[3]The model is general in nature and as such includes control volumes and terms not relevant to this particular device.

Table 1: Calibration goodness-of-fit metrics

	average error	**rms error**	**max error**
ε_{el}	0.4%	0.6%	1.2%
$\dot{N}_{air}$	2.3%	2.8%	5.6%
$(UA)_{eff}$	1.9%	2.1%	3.2%
Heat exchanger condensation	11%	12%	21%
η_{PCU}	0.1%	0.2%	0.2%
$q_{FCPM-to-dilution}$	3.2%	3.9%	7.7%
$q_{skin-loss}$	$\pm$ 20% of nominal value		

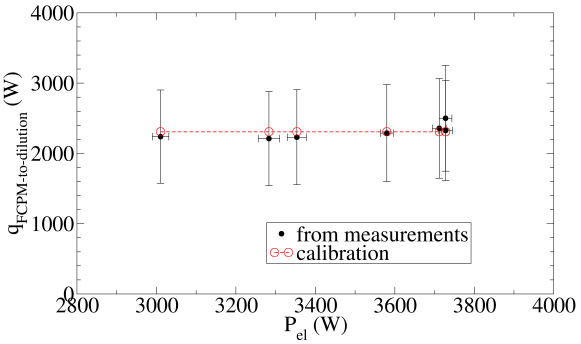

Figure 2: $q_{FCPM-to-dilution}$ calibration versus measurement for calibration experiments

uncertainty rather than goodness-of-fit metrics are presented for the $q_{skin-loss}$ term of equation 1 since it was determined from a single experiment during which infrared images were captured of the cogeneration device's external surfaces. These were used to estimate surface temperatures and classic heat transfer relations were used to estimate the free convection and longwave radiation losses.

Figures 1 and 2 and Table 1 demonstrate that the calibrations of the individual terms of the model accurately represent the calibration data. Worthy of note are the significant uncertainties associated with predicting condensation in the heat exchanger, as well as with the dilution and skin loss heat transfer terms.

VALIDATION APPROACH

Methodology

The validation of building simulation programs is a complex and challenging field that has existed almost as long as building simulation itself. Extensive efforts have been conducted under the auspices of the IEA, ASHRAE, the European Committee for Standardization (CEN), and others to create methodologies, tests, and standards to verify the accuracy and reliability of building simulation programs. Notable examples include Jensen (1993); Lomas et al. (1994); Judkoff and Neymark (1995) and CEN (2004).

In addition to providing consistent methods for comparing predicted results from simulation programs, these initiatives have proven effective at diagnosing errors: inadequacies of simplified mathematical models at representing the thermodynamic processes occurring in reality; mathematical solution inaccuracies; and coding errors (bugs). A pragmatic approach composed of three primary validation constructs to investigate these errors has been widely accepted (Judkoff and Neymark, 1995): analytical verification, empirical validation, and comparative testing.

The second are third methods have been employed to validate the fuel cell cogeneration model. Prior to empirically validating the model, comparative testing was performed to verify the model implementations. The first method, analytical validation, has not been employed due to the complex nature of the devices and the lack of appropriate analytic solutions for the relevant thermodynamic processes.

A general principle applies to all three of these validation constructs. The simpler and more controlled the test case, the easier it is to identify and diagnose sources of error. Realistic cases are suitable for testing the interactions between algorithms, but are less useful for identifying and diagnosing errors. This is because the simultaneous operation of all possible error sources combined with the possibility of offsetting errors means that good or bad agreement cannot be attributed to program validity.

Comparative testing

The model has been independently implemented into five simulation platforms. This provided a unique opportunity to apply inter-model comparison testing to diagnose mathematical solution and coding errors. A suite of 50 test cases, each carefully constructed to isolate a specific aspect of the model, was created (Beausoleil-Morrison et al., 2006a). Collectively these test cases examine every aspect of the model and exercise each line of its source code implementations.

The comparison of simulation predictions between the five programs revealed numerous solution and coding errors that were subsequently addressed. As a result, this exercise has verified the implementations of the model: it can be stated with a high-degree of confidence that the implementations are now error free. Consequently in conducting the empirical validation work, any discrepancies between simulation predictions and measurements could be attributed to inadequacies in the mathematical model or to the calibration of its inputs.

EMPIRICAL VALIDATION

Time-step comparisons for one experiment

Four boundary conditions fully define the operational state of the cogeneration device:

- The AC power production (see P_{AC} in equation 3).
- The flow rate of water through the heat exchanger (see $\dot{N}_w$ in equation 6).
- The temperature of the cold water at the heat exchanger inlet (see T_{w-in} in equation 2).
- The temperature of the air supplied to the FCPM

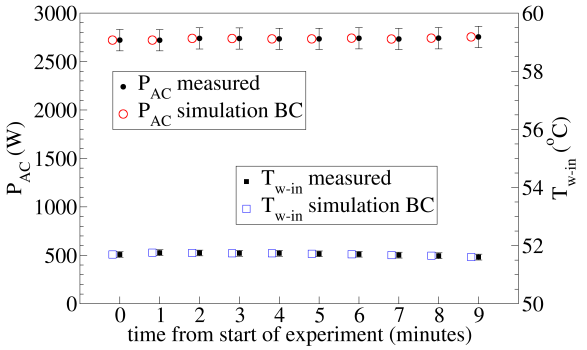

Figure 3: Equivalencing simulation boundary conditions to replicate measurements

(see the $\dot{H}_{air}$ term in equation 1).

These boundary conditions were maintained as constant as possible during each of the 16 validation experiments. Instantaneous measurements of P_{el}, $\dot{N}_{air}$, and $\dot{N}_{fuel}$ were taken every second and the averages over the minute were logged to file. All other measurements were taken every 15 seconds and the minutely averages logged. Figure 3 plots the one-minute averages of two of the boundary conditions (P_{AC} and T_{w-in}) over the 10-minute duration of one of the validation experiments. The error bars in the figure represent the instrumentation bias errors.

An ESP-r (ESRU, 2005) simulation was configured to replicate this experiment. The boundary conditions supplied to ESP-r were equivalenced to the measurements and a simulation conducted with a 1-minute time-step. This boundary condition equivalencing is illustrated in Figure 3. There is a slight time shift between the measurements and the simulation: the simulation was executed at the top of each minute whereas the experimental data were logged a few seconds past the top of each minute.

By equivalencing the boundary conditions, direct comparisons could then be made between the ESP-r simulation results and the measurements. In keeping with the accepted validation methodology's tenet of simplicity, the FCPM's net DC power production (P_{el}) is first compared. P_{el} is calculated with equations 3 and 7 using the u_i coefficients and subject to the P_{AC} boundary condition. Therefore, disagreement between simulation's predictions and measurements would indicate a problem with these aspects of the model and/or the calibration of the u_i coefficients.

The top-left corner of Figure 4 compares the simulations to the measurements. As can be seen, the simulation predictions agree with the measurements within the instrumentation bias error at most of the 10 1-minute intervals. The exception occurs at both the beginning and end of the experiment, where the simulation produces a slightly greater variation in P_{el} from one time-step to the next. (Note the scale of the y-axis.) This slight disagreement was determined to be the result of the iterative solution procedure employed in the ESP-r implementation of the model. Notwithstanding, the average, rms, and maximum deviation between the simulation predictions and measurements indicates excellent agreement overall (see Table 2): the maximum deviation is less than 1%.

Table 2: Goodness-of-fit metrics for time-step simulation predictions for one validation experiment

	average error	**rms error**	**max error**
P_{el}	0.3%	0.4%	0.8%
$\dot{N}_{fuel}$	2.2%	2.2%	2.9%
$(UA)_{eff}$	1.4%	1.7%	3.5%
q_{HX}	6.7%	6.7%	8.0%

The comparisons illustrated in Figure 4 involve greater interactions between algorithms (i.e. less simplicity) as one moves from left to right and from top to bottom. The top-right corner compares the simulation's predictions of the fuel consumption to the measurements. This examines the same aspects of the model as the preceding P_{el} comparison, in addition to equations 4 and 5 and the ε_i empirical coefficients (refer to the earlier discussion on *solution procedure*). The simulation predictions agree with the measurements within the instrumentation bias error (only 2% of the measured value for this experiment) at a number of the 10 1-minute intervals and the goodness-of-fit metrics indicate an excellent prediction overall (see Table 2).

The bottom-left corner of Figure 4 compares the simulation's predictions of the heat exchanger's $(UA)_{eff}$ value to the measurements. This examines the validity of the form of equation 6 and the $hx_{s,i}$ coefficients. In addition, it stresses the aspects of the model that establish $\dot{N}_g$. The simulation predictions agree with the measurements within the instrumentation bias error at each of the 10 1-minute intervals. The goodness-of-fit metrics are similar in magnitude to those for the calibration of the $hx_{s,i}$ coefficients (see Table 1).

The bottom-right corner of Figure 4 compares the simulation's predictions of the useful thermal output (q_{HX}) to the measurements. This examines the combined influence of most aspects of the model. Of particular significance is the large uncertainty associated with the $q_{skin-loss}$ and $q_{FCPM-to-dilution}$ terms of the equation 1 energy balance. As can be seen in the figure, the simulation predictions lie outside the measurement bias uncertainty at all points. However, the goodness-of-fit metrics given in Table 2 are reasonable given the uncertainty associated with the calibration of the two aforementioned heat loss terms: the maximum deviation between simulation predictions and the heat flow derived from measurements is 8%.

Time-averaged comparisons for 16 experiments

The 16 validation experiments varied in duration from 10 minutes to over 10 hours (long experiments were required when condensation formed in the heat ex-

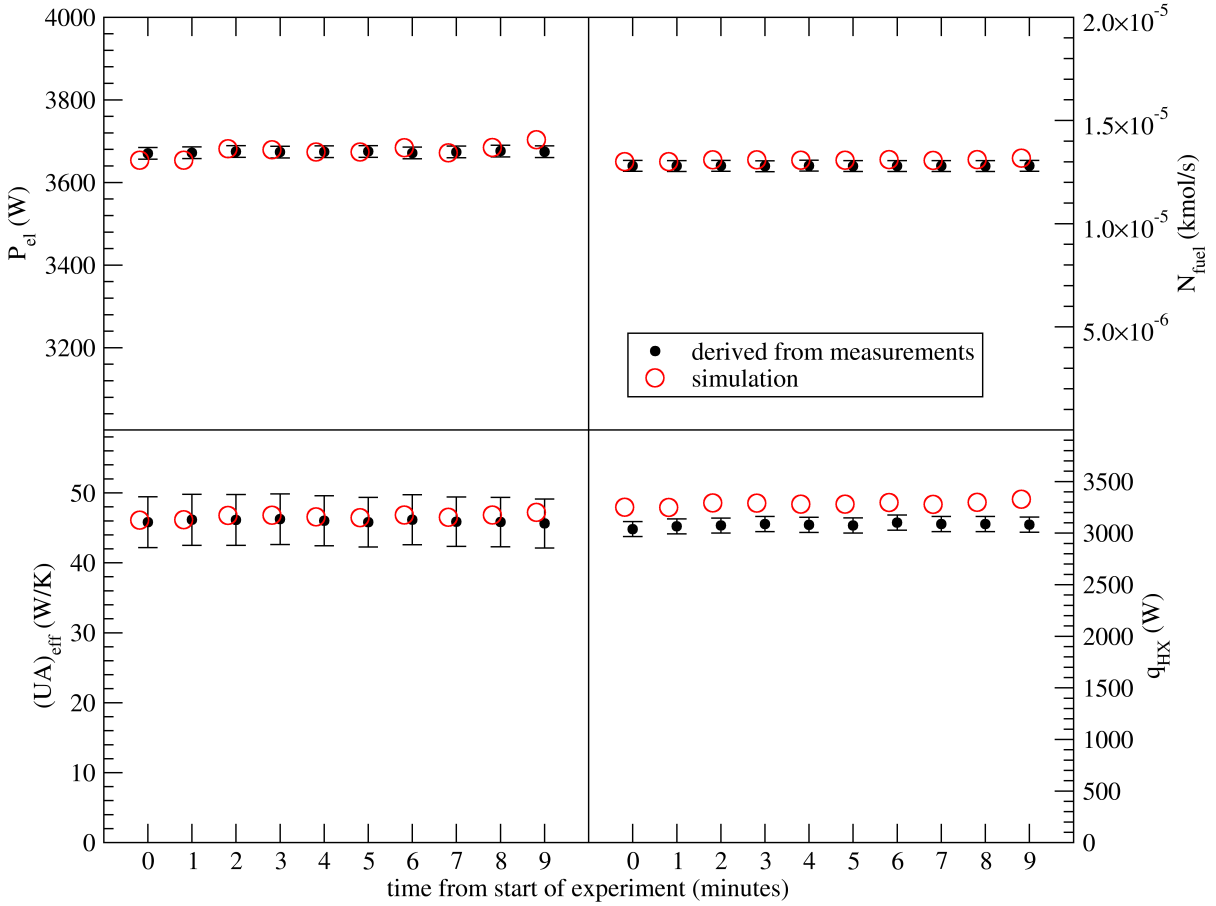

Figure 4: Time-step comparisons of four key simulation predictions for one experiment

changer). The near-constant boundary conditions were time-averaged over each experiment and an ESP-r simulation was configured to equivalence these conditions. This resulted in simulation predictions for 16 sets of time-averaged boundary conditions. Averages were then formed of the derived quantities from the measurements.

These comparisons are illustrated in Figure 5. The quantities derived from the measurements are plotted along the x-axis while the simulation predictions are plotted on the y-axis. The diagonals represent the line of perfect agreement. The error bars in the x-direction represent the uncertainty at the 95% confidence level of the time-averaged quantities derived from the measurements. The goodness-of-fit metrics are presented in Table 3.

In general terms, the simulation predictions deviate further from the measurements as complexity increases. Moving from left to right on the graph and from top to bottom involves greater interaction between algorithms and this affords the possibility of error propagation. It appears from the bottom-right corner of Figure 5 that there may be a systematic bias in the q_{HX} predictions. In fact, a number of the predictions lie within or just outside of the uncertainty bars. The four experiments in which water vapour from the gas stream condensed in the heat exchanger produced the greatest values of

Table 3: Goodness-of-fit metrics for simulation predictions for the 16 validation experiments

	average error	**rms error**	**max error**
P_{el}	0.2%	0.2%	0.5%
$\dot{N}_{fuel}$	1.2%	1.9%	6.1%
$(UA)_{eff}$	5.4%	6.0%	9.5%
q_{HX}	7.9%	8.4%	12.2%
η_{net-AC}	1.2%	1.8%	5.8%
η_{th}	8.5%	8.8%	13%
η_{cogen}	5.3%	5.6%	8.9%

q_{HX}. These experiments show some of the greatest deviation between simulation results and measurements. As explained earlier there is considerable uncertainty associated with the calibration of this aspect of the model.

Furthermore, the error bars in the bottom-right of Figure 5 likely underestimate the true experimental uncertainty. The uncertainty at the 95% confidence interval was calculated through the propagation of bias errors and measurement precision indices through a root-sum-square method (Moffat, 1988). The bias errors were established mainly based upon instrumentation specifications. As such, the uncertainty bars in the figure represent the errors associated with two type-T thermocouples (bias errors of 0.1^oC) that measured

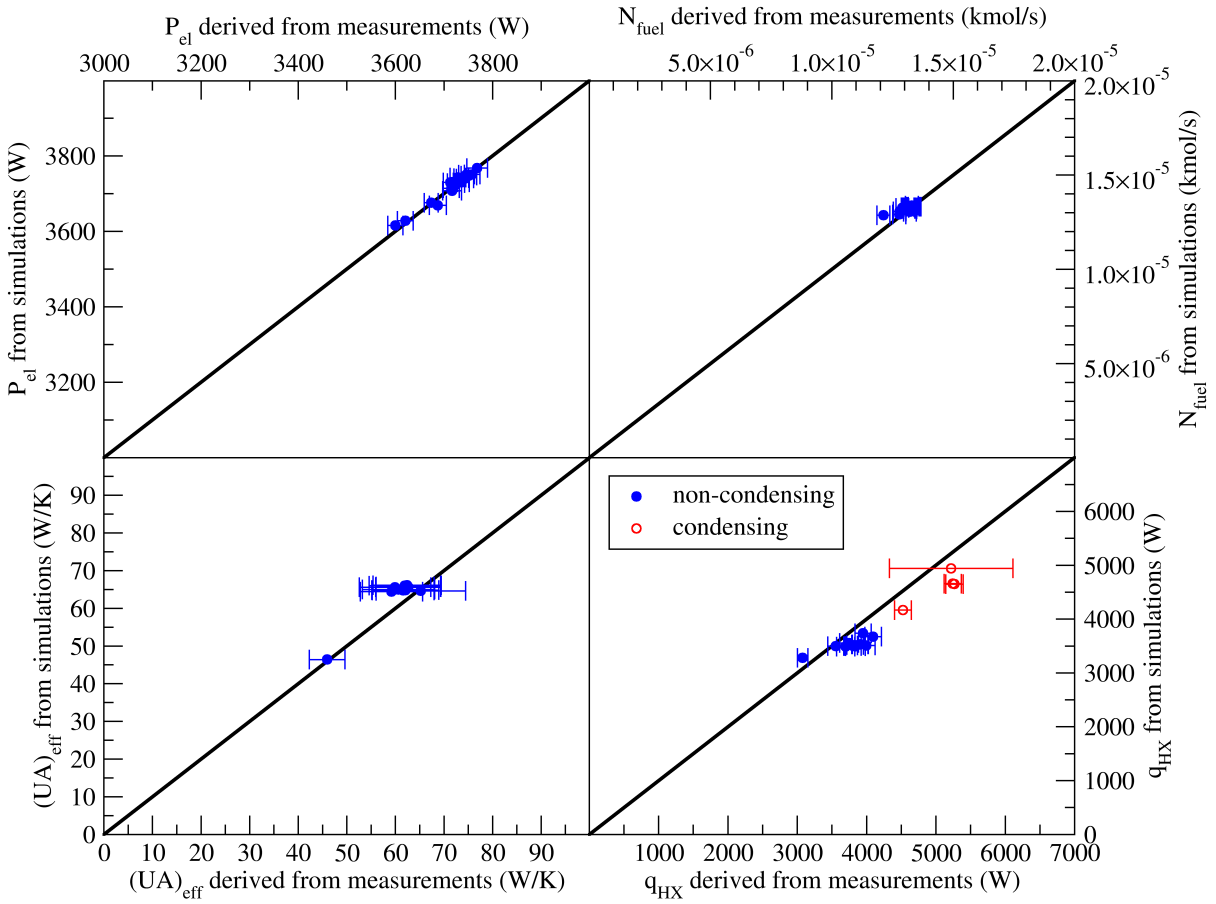

Figure 5: Time-averaged comparisons of four key simulation predictions for the 16 validation experiments

T_{w-in} and T_{w-out} and a water flow meter to measure $\dot{N}_w$(bias error of ~2%). In contrast, the simulation predictions are dependent upon the calibration of equation 6. This calibration relies upon the aforementioned instruments as well as two type-K thermocouples (bias errors of 2.2^oC) that measured $T_{FCPM-cg}$ and T_{g-out} (refer to equation 2). Analysis of the measured data revealed an inconsistency in the measurements of these four temperatures, $\dot{N}_w$, and $\dot{N}_g$: the derived heat flow from the heat exchanger's gas stream was often less than the derived heat flow to the water stream. This indicates that the instrumentation bias errors may have in fact been greater than the manufacturer specifications. Or, that placement of one or more of the thermocouples may have biased the readings, i.e. it may not have been reading the intended state point. Taken in this context, it can be stated that the goodness-of-fit metrics indicate reasonable agreement between simulation results and measurements over the 16 validation experiments.

The final check on the model's validity is made through examining the predictions of three key outputs, the net efficiencies for electrical, useful thermal, and total output from the cogeneration device,

$$\eta_{net-AC} = \frac{P_{AC}}{\dot{N}_{fuel} \cdot LHV_{fuel}} \quad (9)$$

$$\eta_{th} = \frac{q_{HX}}{\dot{N}_{fuel} \cdot LHV_{fuel}} \quad (10)$$

$$\eta_{cogen} = \eta_{net-AC} + \eta_{th} \quad (11)$$

These three efficiency values would be of prime importance in a simulation-based assessment of the performance of residential cogeneration systems. Their calculation depends upon the interaction of all aspects of the model. The comparison of the simulation predictions of these quantities with the values derived from the measurements are illustrated in Figure 6 and the goodness-of-fit metrics are presented in Table 3. As can be seen, simulation predictions of the electrical efficiency are in better agreement than those for the thermal efficiency. However, for the reasons elaborated above it can be stated that the ability of the model to predict performance is quite reasonable.

CONCLUSIONS

This paper has demonstrated the validity of a mathematical model—and its calibration—for simulating the performance of fuel cell cogeneration systems. Pertinent aspects of the mathematical model were described and the methods used to calibrate the model (i.e. establish its inputs) using data gathered through 45 experiments conducted with a prototype solid-oxide fuel-cell (SOFC) cogeneration system were presented. The methodology used to validate the model and its implementation into building simulation programs was then elaborated. This described how inter-model compara-

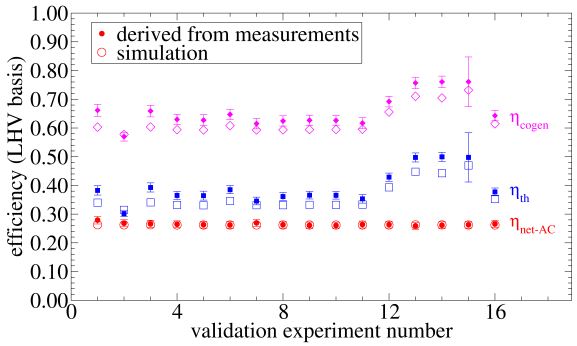

Figure 6: Time-averaged comparisons of efficiencies for the 16 validation experiments

tive testing was used to eliminate coding and solution errors. The paper then described how measured data from 16 experiments (disjunct from the 45 experiments used to calibrate the model) were used to empirically validate the model and its calibration. It showed how simulations were equivalenced with experimental conditions and how measured values and quantities derived from the measurements were compared to simulation predictions. These comparisons spanned a range of model parameters, progressing from the simplest case in which only a small subset of the model was exercised, to the complex which involved the concurrent operation and interaction of all aspects of the model.

The paper identified the aspects of the model with the greatest uncertainty, that is the calculation of parasitic thermal losses and the condensation of the exhaust gas' water vapour within the heat recovery device. The paper explained how this uncertainty could propagate errors into the simulation predictions of the useful thermal output. In addition, an inconsistency in the measurements related to the heat recovery device were revealed, and probable explanations were postulated. This observation exacerbated comparisons between simulation predictions of the useful thermal output and the values derived from measurements. Notwithstanding, acceptable to excellent agreement between simulation predictions and measurements was found for numerous key parameters and over the range of the 16 experiments. The conclusion is drawn that the model fairly represents the performance of fuel cell cogeneration devices and their sub-systems and that the calibrated model produces valid predictions of the performance of the prototype SOFC system.

In the future it is hoped that the model calibration procedure will be repeated for other fuel cell cogeneration devices. In addition, simulations will be performed will the calibrated model to predict the performance of the prototype SOFC system under different operating scenarios and coupled to houses with various thermal and electrical demand characteristics. These results will provide insight into the potential benefits of this nascent technology.

ACKNOWLEDGEMENTS

The work described in this paper was undertaken as part of IEA/ECBCS Annex 42 (www.cogen-sim.net). The Annex is an international collaborative research effort and the authors gratefully acknowledge the indirect or direct contributions of the other Annex participants. The contributions of Ms. Kathleen Siemens in analyzing the measured data are greatly appreciated.

REFERENCES

Beausoleil-Morrison, I., Griffith, B., Vesanen, T., Lerson, S., and Weber, A. (2006a). A case study demonstrating the utility of inter-program comparative testing for diagnosing errors in building simulation programs. In *Proc. eSim 2006*, pages 181–188, Toronto Canada.

Beausoleil-Morrison, I., Schatz, A., and Maréchal, F. (2006b). A model for simulating the thermal and electrical production of small-scale solid-oxide fuel cell cogeneration systems within building simulation programs. *J HVAC&R Research*, 12(3a):641–667.

Beausoleil-Morrison, I., Siemens, K., and Oikawa, S. (2006c). On methods for calibrating the heat exchanger of a model for simulating the thermal and electrical production of small-scale solid-oxide fuel cell cogeneration systems. In *Proc. 7th Int. Conf. on System Simulation in Buildings*, Liège Belgium.

CEN (2004). *prEN ISO 13791: Thermal Performance of Buildings Calculation of Internal Temperatures of a Room in Summer without Mechanical Cooling—General Criteria and Validation Procedures*. ISO/FDIS 13791:2004, Brussels Belgium.

ESRU (2005). The ESP-r system for building energy simulations: User guide version 10 series. Technical Report U05/1, University of Strathclyde, Glasgow UK.

Jensen, S., editor (1993). *Validation of Building Energy Simulation Programs, Part I and II*. PASSYS Subgroup Model Validation and Development. EUR 15115 EN.

Judkoff, R. and Neymark, J. (1995). *International Energy Agency Building Energy Simulation Test (BESTEST) and Diagnostic Method*. IEA/ECBCS Annex 21 & IEA/SHC Task 12 Report.

Knight, I. and Ugursal, V. (2005). *Residential Cogeneration Systems: A Review of the Current Technologies*. IEA/ECBCS Annex 42 Report. ISBN No. M154-1/2005E.

Lomas, K., Eppel, H., Martin, C., and Bloomfield, D. (1994). *Empirical Validation of Thermal Building Simulation Programs Using Test Room Data, Volume 1: Final Report*. IEA/ECBCS Annex 21 & IEA/SHC Task 12.

Moffat, R. (1988). Describing the uncertainties in experimental results. *J Experimental Thermal and Fluid Science*, 1:3–17.